Int J Fract (2019) 215:175–182
https://doi.org/10.1007/s10704-018-00337-7

BRIEF NOTE

Theoretical approach to determine dynamic fatigue strength characteristics of ceramics under variable loading rates on the basis of SCG concept

Shinya Matsuda

Received: 21 August 2018 / Accepted: 27 November 2018 / Published online: 8 January 2019

Abstract This paper presents a theoretical approach to determine the dynamic fatigue strength characteristics of ceramics under variable loading rates on the basis of the slow crack growth (SCG) concept. First, a probabilistic effective inert strength model was derived on the basis of the SCG concept in conjunction with the Weibull distribution for ceramics subjected to multi-stage loading. Second, a four-point bending test was conducted on Al_2O_3 under constant and two-stage variable loading rates, and the fracture surface was then observed. The experimental data that depend on loading rates can be unifiedly evaluated after converting the data to the effective inert strength, obeying the three-parameter Weibull distribution. In addition, the Weibull plots of the inert strength, which were calculated from the inclusion size on the fracture surface using the grain fracture model, showed good agreement with the three-parameter Weibull distribution for the converted effective inert strength. These analytical results theoretically indicate that dynamic fatigue under variable loading rates occurs by obeying SCG at the inclusion. Further, the inert strength and its scatter depend on the size and distribution of inclusions.

S. Matsuda (✉)
Area in Advanced Materials Science, Department of Engineering and Design, Faculty of Engineering and Design, Kagawa University, 2217-20 Hayashi-cho, Takamatsu, Kagawa 761-0396, Japan
e-mail: matsuda@eng.kagawa-u.ac.jp

Keywords Ceramics · Variable loading rate · Dynamic fatigue strength · SCG · Inclusion size · Inert strength

1 Introduction

The brittle fracture of ceramics occurs owing to various defects such as internal crack-like defects, void, coarse grains, impurities, inclusion, and processing flaws. The strength of ceramics is determined by the fracture toughness and the largest defect size (Ritter 1995) in the various defects. It is well known that the strength depends on the loading time because fracture occurs owing to slow crack growth (SCG) at the largest defect (Evans 1980). Research on fatigue fracture has been actively conducted since the 1970s. The SCG concept was developed by Evans and Wiederhorn, which is a classical concept for predicting strength and life. The following studies were conducted on the basis of the SCG concept: cyclic fatigue crack propagation (Evans and Fuller 1974; Evans et al. 1975; Evans and Lange 1975), dynamic (Evans and Johnson 1975) and static (Wiederhorn and Bolz 1970) fatigue strength properties at room and high temperatures, probabilistic relationships between stress and life in conjunction with the Weibull distribution (Evans and Wiederhorn 1974a), and life prediction (Evans and Wiederhorn 1974b). In addition to these, several researchers have applied the SCG concept to the analysis of the dynamic and static (Ritter and Humenik 1979; Seshadri et al. 1982; Phani 1988; Breder 1995; Pan et al. 1998; Choi et al. 2005;

Pfingsten and Glien 2006; Teixeira et al. 2007; Matsuda and Watanabe 2011; Matsuda and Ogi 2017), cyclic (Guiu et al. 1991; Okabe and Ikeda 1991; Zhu et al. 2004), and thermal fatigue properties (Hasselman et al. 1975; Kamiya and Kamigaito 1982; Ogi and Ito 2011) of various ceramics. It should be noted that these analyses were carried out on experimental data obtained from fatigue tests under a constant loading rate, static, and stress amplitude loadings. To assure the strength reliability of a system using ceramics, it is necessary to investigate fatigue properties under not only these constant loading conditions but also variable loading conditions. Previous studies on fatigue properties under variable loading conditions include Gilberta and Ritchiea (1998) and Choi and Horibe (1993), who investigated the propagation behavior of cyclic fatigue cracks under variable stress amplitude loadings. Hoshide et al. (1988) analyzed the cyclic fatigue life under two-step variable cyclic loading on the basis of the SCG concept. Siegmund (2004) numerically analyzed the growth of transient fatigue cracks using an irreversible cohesive zone model. Ogi et al. (2010) predicted the transverse crack density under two-step variable cyclic loadings using a probabilistic SCG model to evaluate brittle matrix cracking in carbon fiber reinforced plastics (CFRP) laminates. However, the dynamic fatigue strength characteristics under variable loading rates were not experimentally and theoretically investigated.

The purpose of this study is to theoretically determine the dynamic fatigue strength characteristics of ceramics under variable loading rates on the basis of the SCG concept. First, a probabilistic effective inert strength model was derived on the basis of the SCG concept, in conjunction with the Weibull distribution for ceramics subjected to multi-stage loading. Next, experimental data obtained from the four-point bending (FPB) test of Al_2O_3 under two-stage variable loading rates were analyzed using the model. Finally, the relationship between the effective inert strength determined from experimental data and inclusion size of the fracture occurring in ceramics was theoretically discussed.

2 Modeling

In this modeling, the cumulative crack propagation of SCG during multi-stage variable loading of p ($1 \leq \mathrm{j} \leq \mathrm{p}$) steps is considered. When stress $\sigma_\mathrm{j}(t)$ (period time t_j) is applied to a brittle body with a crack in the jth stage, the stress intensity factor K_I at mode I of a crack of length a is expressed as

$$K_\mathrm{I} = Y\sigma_\mathrm{j}(t)\sqrt{a} \tag{1}$$

where Y denotes a constant that depends on the geometry of the crack. Then, the crack propagation rate v for SCG is given as (Evans 1980)

$$v = \frac{\mathrm{d}a}{\mathrm{d}t} = C\left(\frac{K_\mathrm{I}}{K_\mathrm{IC}}\right)^n \tag{2}$$

where n, K_IC, and C denote the crack propagation index, fracture toughness, and material constant which is v at K_IC, respectively. Directly integrating Eq. (2) using Eq. (1) yields

$$a_{\mathrm{j}-1}^{-\lambda} - a_\mathrm{j}^{-\lambda} = C\lambda\alpha^n\sigma_{\mathrm{max,j}}^n t_{\mathrm{eff,j}} \tag{3}$$

where $a_{\mathrm{j}-1}$, a_j, and $\sigma_{\mathrm{max,j}}$ denote the crack length at the end of the j–1th stage, the crack length at the end of the jth stage, and the maximum stress at the jth stage, respectively, α and λ equal Y/K_IC and $(n-2)/2$, respectively, and

$$t_{\mathrm{eff,j}} = \int_0^{t_\mathrm{j}}\left(\frac{\sigma_\mathrm{j}(t)}{\sigma_{\mathrm{max,j}}}\right)^n \mathrm{d}t \tag{4}$$

is the effective loading time at the jth stage, which is the time obtained assuming that $\sigma_{\mathrm{max,j}}$ is statically loaded. The summation of Eq. (3) with respect to j from 1 to p yields

$$a_0^{-\lambda} - a_\mathrm{p}^{-\lambda} = C\lambda\alpha^n\sum_{\mathrm{j}=1}^{\mathrm{p}}\sigma_{\mathrm{max,j}}^n t_{\mathrm{eff,j}} \tag{5}$$

where a_0 and a_p denote the crack length at the end of the 0th stage (i.e., the initial crack length) and the crack length at the end of the pth stage, respectively.
a_0 is related to K_IC and the inert strength S_i using Eq. (1) as

$$a_0 = \left(\frac{K_\mathrm{IC}}{YS_\mathrm{i}}\right)^2. \tag{6}$$

When unstable crack growth occurs at the end of the pth stage, a_p is expressed as

$$a_\mathrm{p} = \left(\frac{K_\mathrm{IC}}{Y\sigma_{\mathrm{max,p}}}\right)^2. \tag{7}$$

Substituting Eqs. (6) and (7) into Eq. (5), the effective inert strength S_i^*, which is a function corresponding to the maximum stress and the effective loading time in all the stages, leads to

$$S_i^* = \sigma_{max,p} \left\{ 1 + g_o \sigma_{max,p}^{-2\lambda} \sum_{j=1}^{p} \sigma_{max,j}^{n} t_{eff,j} \right\}^{1/2\lambda} \tag{8}$$

where g_o equals $C\lambda\alpha^2$; when p = 1, Eq. (8) becomes (Matsuda and Ogi 2017)

$$S_i^* = \sigma_{max} \left\{ 1 + g_o \sigma_{max}^2 t_{eff} \right\}^{1/2\lambda}. \tag{9}$$

Assuming the weakest link model, the brittle fracture of ceramics including initial cracks with various sizes occurs at one of the largest cracks. It should be noted that a lower limit for the inert strength S_{th} must exist because there is an upper limit of the crack length a_{th} in the cracks. When the inert strength S_i obeys the three-parameter Weibull distribution, replacing S_i with the effective inert strength S_i^* in Eq. (8) gives the fracture probability F as

$$F = 1 - \exp\left[-\left(\frac{S_i^* - S_{th}^*}{S_o} \right)^m \right] \tag{10}$$

where S_{th}^*, m, and S_o denote the location, shape, and scale parameters, respectively. Incidentally, $S_{th}^* \approx 0$ in Eq. (10) gives the two-parameter Weibull distribution as

$$F = 1 - \exp\left[-\left(\frac{S_i^*}{S_o} \right)^m \right]. \tag{11}$$

Therefore, in the case of the SCG-controlled time-dependent fracture, the strength data obtained from tests conducted under single and multi-stage variable loadings can be unifiedly evaluated by Weibull analysis of the effective inert strength converted using Eq. (8).

3 Experimental procedures

3.1 Specimen

The specimen used in the experiment was Al_2O_3 (Referceram AL1, JFCC) with a rectangular cross section (^{w}4 mm × ^{h}3 mm × ^{L}40 mm). The average surface roughness was measured as 0.36 µm. The mechanical properties are listed in Table 1. The fracture toughness K_{IC}^* was measured through a three-point bending test conducted for specimen-introduced pop-in crack at a crosshead speed (CHS) of 0.5 mm min^{-1} based on the single edge pre-cracked beam (SEPB) method

Table 1 Mechanical properties of Al_2O_3

Bulk density ρ (Mg/m^3)	Young's modulus E (GPa)	Mean grain size d_o (µm)	Fracture toughness K_{IC}^* (MPa$\sqrt{m}$)
3.93	380	5.3	4.4

Fracture toughness K_{IC}^* was measured using the SEPB (single edge pre-cracked beam) method

of the ISO 15732 or the Japanese Industrial Standard (JIS) R1607. The K_{IC}^* denotes the fracture toughness for a long crack, which is different from the true fracture toughness K_{IC} for a small crack. In addition, it should be noted that the K_{IC}^* measured from the SEPB method slightly depends on the CHS due to slow crack growth (Quinn et al. 1992; To et al. 2018).

3.2 FPB test under two-stage variable loading rates

A universal testing machine (Autograph AG-10TE, SHIMADZU) set up as a load cell with a capacity of 5 kN, including a jig for the FPB test (under span L_1 = 30 mm, upper span L_2 = 10 mm), was used as the test machine for the experiments. The FPB test was conducted under a two-stage variable loading rate (2S-VLR) test by switching the CHS at room temperature in air. The CHS at the stage-switching loading stress in the 2S-VLR test is as follows: Condition I: 0.05 mm min^{-1} → 0.005 mm min^{-1}, II: 0.05 mm min^{-1} → 1 mm min^{-1}, and III: 0.05 mm min^{-1} → 10 mm min^{-1}. The average stress rates for CHSs of 0.005, 0.05, 1, and 10 mm min^{-1} are 0.264, 2.75, 60.5, and 620 MPa s^{-1}, respectively. The stage-switching loading stress was determined as the fracture stress at a fracture probability of 40%, which was calculated from the two-parameter Weibull distribution of the fracture stress obtained from the FPB test under a constant loading rate (CLR) test at a CHS of 0.05 mm min^{-1}. The FPB fracture stress σ_{max} for these tests was calculated as

$$\sigma_{max} = \frac{3P(L_1 - L_2)}{2wh^2} \tag{12}$$

where P, w, and h denote the fracture load, width, and height of the specimen, respectively.

4 Results

Figure 1 shows the Weibull plots of the fracture stress σ_{max} obtained from the CLR test at a CHS of

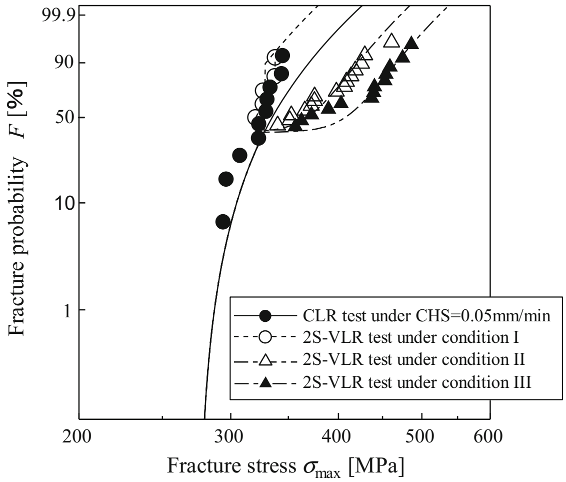

Fig. 1 Weibull plots of fracture stress obtained in CLR test at CHS $= 0.05\,\mathrm{mm\,min^{-1}}$ and 2S-VLR test, and curves predicted from Eqs. (8) and (10)

$0.05\,\mathrm{mm\,min^{-1}}$ and 2S-VLR tests, where the stage-switching loading stress for the 2S-VLR tests was 320 MPa (curves in Fig. 1 are explained in Sect. 5.2). The fracture probability F is determined using the median rank method as follows:

$$F = \frac{i - 0.3}{N + 0.4} \tag{13}$$

where i is the modified order of σ_{max} for N data points. The value of σ_{max} under condition I was slightly lower than that in the CLR test. On the other hand, σ_{max} values under conditions II and III were higher than those in the CLR test and increases with an increase in the switching CHS.

Figure 2 shows scanning electron microscope (SEM) images of the fracture surface near the maximum stress after the 2S-VLR tests under conditions II and III. Although mirror, mist, and hackle were obviously observed in the fracture surface of glass and silicon nitride (Tanaka et al. 2002; Matsuda and Watanabe 2011), the characteristic fracture surface was not observed in these fracture surfaces. The fracture surfaces aspect did not vary under different test conditions, and inclusion was observed in either case, which was the same as the fracture surface (Matsuda and Ogi 2017) in the CLR test. From the above results, it can be presumed that brittle fracture in CLR and 2S-VLR tests occurs at an inclusion. It should be noted that the fracture stress calculated using Eq. (12) may be slightly overestimated as it is assumed that the fracture occurs

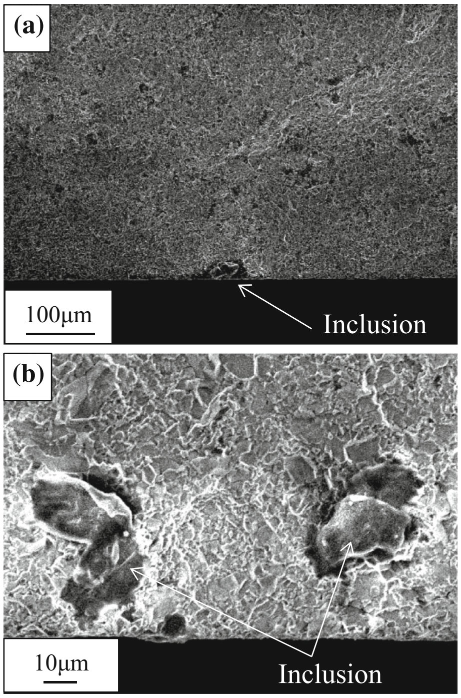

Fig. 2 SEM images of fracture surfaces obtained in 2S-VLR tests under conditions **a** II and **b** III

at the surface although Fig. 2 shows otherwise. In this study, the fracture stress was approximately calculated using Eq. (12) because the position of the observed inclusion was approximately 20 µm from the surface (see Fig. 2b).

5 Discussion

5.1 Weibull plots of effective inert strength converted using data from CLR and 2S-VLR tests

Data from the CLR and 2S-VLR tests were converted to the effective inert strength S_i^* using Eq. (8) and the SCG parameters of $n = 21.1$ and $g_o\left(= C\lambda\alpha^2\right) = 2.54 \times 10^{-3}\,\mathrm{MPa^{-2}\,s^{-1}}$ in Table 2. The CLR test data was obtained under a wide range of CHSs from 1000 to $0.005\,\mathrm{mm\,min^{-1}}$ at room temperature in air; then, the SCG parameters were determined from the data (see the "Appendix" and Matsuda and Ogi 2017).

Figure 3 shows the Weibull plots of S_i^*. Table 2 lists the two and three Weibull parameters of Eqs. (10) and (11) analyzed from the Weibull plots of S_i^*. The Weibull parameters were analyzed using the least

Table 2 SCG parameters and Weibull parameters in Eqs. (10) and (11) of the effective inert strength for data in CLR and 2S-VLR tests

g_o ($\mathrm{MPa}^{-2}\,\mathrm{s}^{-1}$)	2.54×10^{-3}
n	21.1
Eq. (10)	
S_o (MPa)	115.6
m	2.71
S^*_{th} (MPa)	390.7
Eq. (11)	
S_o (MPa)	511
m	14.8

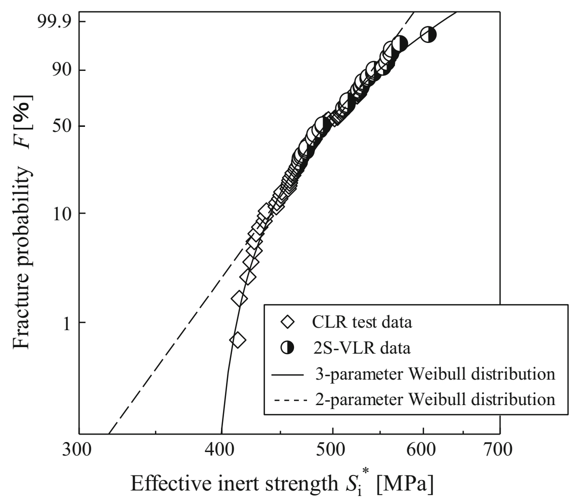

Fig. 3 Weibull plots of effective inert strength converted from data obtained in CLR and 2S-VLR tests, and curves predicted from Eqs. (10) and (11) using the Weibull parameters

squares method and the correlation coefficient method (Sakai and Tanaka 1980), respectively. The lines in Fig. 3 were plotted from Eqs. (10) and (11) using the Weibull parameters. 2S-VLR test data that depend on the variable loading rates shown in Fig. 1 can be unifiedly evaluated on a Weibull probability paper together with the CLR test data, where S^*_i can be approximated by a curved line rather than a straight line, indicating that S^*_i conforms to the three-parameter Weibull distribution. The analytical results support the proposed model for multi-stage variable loading test data, indicating that brittle fracture under VLR obeys SCG.

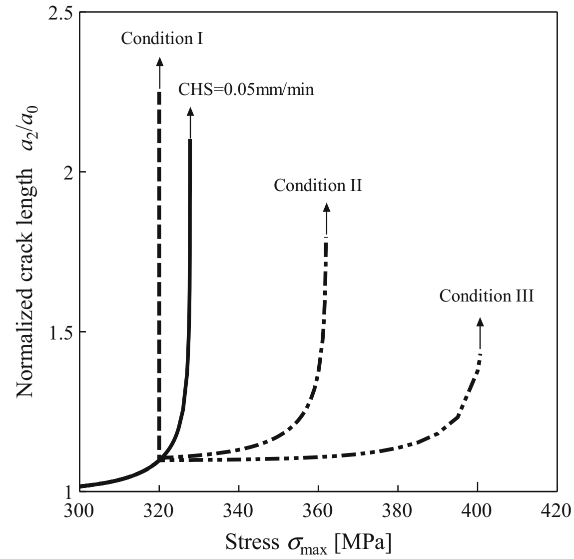

Fig. 4 Calculated crack length during CLR and 2S-VLR tests

5.2 Weibull plots of fracture stress depending on variable loading rates

In this section, variable loading rates dependence of the fracture stress shown in Fig. 1 is discussed. The curves in Fig. 1 were predicted from Eqs. (8) and (10) using the SCG parameters and Weibull parameters for Eq. (10), as presented in Table 2. The predicted curves can accurately reproduce the experimental data. Figure 4 depicts the crack length a_p calculated as p = 2 at each condition using the SCG parameters presented in Table 2, normalized by the initial crack length $a_0 = \left\{K_{IC}/\left(Y S^*_i\right)\right\}^2$. The curves represent the crack length using

$$a_p = a_0 \left\{ 1 - \frac{g_o}{S_i^{*2\lambda}} \sum_{j=1}^{p} \sigma_{max,j}^{n} t_{eff,j} \right\}^{-1/\lambda}, \qquad (14)$$

which is obtained from Eqs. (7) and (8), whereas the arrows indicate the unstable growth predicted using Eq. (7), assuming $Y = \sqrt{\pi}$, $K_{IC} = K^*_{IC}$, and S^*_i is the average of σ_{max} in the CLR test under CHS $=$ 200 mm min^{-1} (see the "Appendix").

The results indicate that when the loading rate after switching is low, such as condition I, the fracture stress decreases slightly compared to that under the loading rate before switching owing to the increase in the critical crack length after SCG. On the other hand, when the loading rate after switching is high, such as conditions II and III, the fracture stress increases compared to that under the loading rate before switching owing to the decrease in the critical crack length after SCG. Therefore, Weibull plots of fracture stress depending on variable loading rates exhibit discontinuous behavior.

5.3 Calculation of the effective inert strength from processing flaw size

It is considered that unstable crack growth occurs when the stress intensity factor reaches the fracture toughness K_{IC} for small crack without stable crack growth owing to the tensile stress acting on a semicircular surface crack or internal circular crack. Then, the constant fracture toughness criterion (LFM model) is given using the inert strength S_i and the equivalent crack length a_{eq} as

$$K_{IC} = S_i\sqrt{\pi a_{eq}}. \tag{15}$$

If the value K_{IC} is given as the fracture toughness K_{IC}^* for long cracks measured by the SEPB method, the fracture stress of a long pre-cracked ceramics can be explained. However, the fracture stress of smooth ceramics, including small initial cracks, cannot be explained (Hoshide and Hiramatsu 1999). Therefore, Usami et al. (1986) proposed a grain fracture model for smooth ceramics as follows:

$$\frac{K_{IC}}{K_{IC}^*} = \frac{\sqrt{1 + r/2a_{eq}}}{1 + r/a_{eq}} \tag{16}$$

where r denotes the grain size at a crack tip. Substituting Eq. (15) into Eq. (16), S_i of smooth ceramics is obtained as

$$S_i = \frac{K_{IC}^*}{\sqrt{\pi a_{eq}}}\frac{\sqrt{1 + r/2a_{eq}}}{1 + r/a_{eq}}. \tag{17}$$

Figure 5 shows the Weibull plots of S_i calculated using Eqs. (15) and (17) and the calculated a_{eq} and curves predicted from Eqs. (10) and (11) using the Weibull parameters listed in Table 2. Then, r in Eq. (17) and K_{IC} in Eq. (15) were given as $2d_o$ (Usami et al. 1986) and K_{IC}^*, respectively, where d_o denotes the mean grain size (see Table 1). In addition, a_{eq} was calculated using the inclusion size observed in the fracture surface in the CLR test and the following equations: $0.226\sqrt{area}$ (for a semicircular surface crack) and $0.399\sqrt{area}$ (for an internal circular crack). The term *area* in the equations denotes the area of these cracks (Usami et al. 1986; Matsuda 2016). A good agreement was observed between the S_i calculated using Eq. (17) and the predicted three-parameter Weibull distribution, including the scatter.

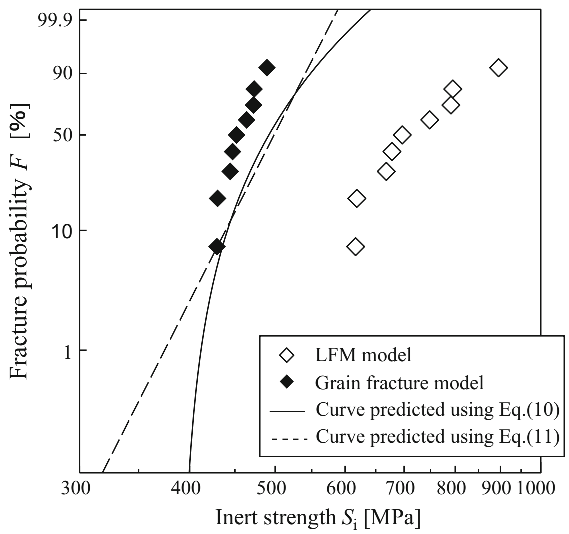

Fig. 5 Weibull plots of S_i calculated using LFM, and grain fracture models and curves predicted using Eqs. (10) and (11). S_i calculated using the grain fracture model showed good agreement with the curve of Eq. (10). The results indicate that when SCG does not occur, brittle fracture occurs at the grain of the crack tip

The results indicate that brittle fracture occurs at the weakest part in the grain located at the tip of the inclusion, irrespective of the variable loading rate. It is concluded that the inert strength and its statistical characteristics are dependent on the size and distribution of inclusions in ceramics.

6 Conclusion

In this study, a probabilistic effective inert strength model, which was derived on the basis of the SCG concept in conjunction with the Weibull distribution for ceramics subjected to multi-stage loadings, was proposed to theoretically determine the dynamic fatigue strength characteristics of ceramics under variable loading rates. The experimental data obtained from the FPB test of Al_2O_3 under constant and two-stage variable loading rates were analyzed using the model. The analytical results indicate that these experimental data that depend on the loading rates can be evaluated in a unified manner by converting the data to the effective inert strength. The effective inert strength obeys the three-parameter Weibull distribution. In addition, the Weibull plots of the inert strength calculated using the grain fracture model from the inclusion size in the fracture surface showed good agreement with the three-parameter Weibull distribution for the converted effective inert strength. From these analyses, it can be concluded that dynamic fatigue fracture under variable loading rates occurs by obeying SCG at the inclusion. Further, the inert strength and its scatter depend on the size and distribution of inclusions.

Acknowledgements I would like to show my greatest appreciation to Prof. K. Ogi (Ehime University, Japan) whose comments and advice were highly valuable throughout the course of my study.

Funding This work was supported by JSPS KAKENHI [Grant Number 17K14563].

Appendix: Determination of SCG parameters

The SCG parameters n and g_o were determined using the $\sigma_{max} - \dot{\sigma}$ plots (loading rate $\dot{\sigma}$) in the CLR test shown in Fig. 6a by rewriting Eq. (9) as follows:

$$y = \ln\left(\frac{S_i^*}{\sigma_{max}}\right) = \frac{1}{n-2}\ln\left(1 + g_o\sigma_{max}^2 t_{eff}\right). \quad (18)$$

The ratio S_i^*/σ_{max} on the left-hand side of Eq. (18) was plotted against $x = \sigma_{max}^2 t_{eff}$. Here, the effective inert strength S_i^* was assumed to be the average of σ_{max} in the CLR test under CHS $= 200\,\text{mm min}^{-1}$, which converges to the inert strength as shown in Fig. 6a, and the effective loading time t_{eff} was calculated using Eq. (4) and the applied stress $\sigma(t) = \dot{\sigma}t$ (period stress $\sigma_{max} = \dot{\sigma}t_f$) as $\sigma_{max}/\{\dot{\sigma}(n+1)\}$. Then, n and g_o were obtained by curve fitting these plots to the equation $y = 1/(n-2)\ln(1 + g_o x)$ using the least squares method, as shown in Fig. 6b. The values of n and g_o were obtained as 21.1 and $2.54 \times 10^{-3}\,\text{MPa}^{-2}\,\text{s}^{-1}$, respectively. The value of n was smaller than $n = 37.5$, which was obtained by Ritter and Humenik (1979). They conducted the CLR test under the loading rate region from 1/10 to 1/100 of the lowest loading rate of the CLR test in this study. Then, n was analyzed by curve fitting the obtained $\sigma_{max} - \dot{\sigma}$ plots to the equation $\sigma_{max} \propto \dot{\sigma}^{1/(n+1)}$, which is obtained on the basis of the SCG concept. On the other hand, on analyzing the S–N diagram in the cyclic fatigue test and the S–t diagram in the static fatigue test, the value of n varied between 21–25 and 36–54, respectively (Guiu et al. 1991). The value of n obtained from the S–N diagram almost agrees with this experimental result. The value of n differs depending on the loading method and the loading rate region.

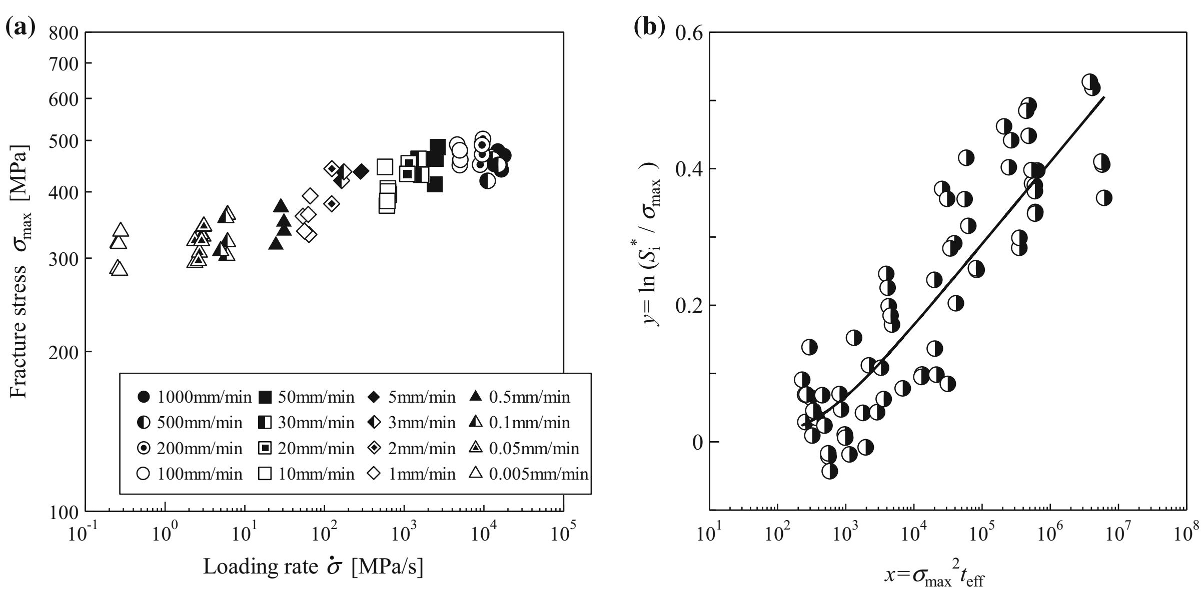

Fig. 6 **a** $\sigma_{max} - \dot{\sigma}$ plots in CLR test data and determination of SCG parameters for **b** measured and fitted values of y versus x in Eq. (18). (Reproduction of Figs. 1 and 3 from Matsuda and Ogi 2017)

References

Breder K (1995) Time-dependent strength degradation of a siliconized silicon carbide determined by dynamic fatigue. J Am Ceram Soc 78(10):2680–2684

Choi G, Horibe S (1993) The influence of variable-amplitude loading on cyclic-fatigue crack growth in silicon nitride. J Mater Sci Lett 12(24):1886–1887

Choi SR, Nemeth NN, Gyekenyesi JP (2005) Exponential slow crack growth of glass and advanced ceramics-dynamic fatigue. Fatigue Fract Eng Mater Struct 28(5):489–497

Evans AG (1980) Fatigue in ceramics. Int J Fract 16(6):485–498

Evans AG, Fuller ER (1974) Crack propagation in ceramic materials under cyclic loading conditions. Metall Trans 5:27–33

Evans AG, Johnson H (1975) The fracture stress and its dependence on slow crack growth. J Mater Sci 10(2):214–222

Evans AG, Lange FF (1975) Crack propagation and fracture in silicon carbide. J Mater Sci 10(10):1659–1664

Evans AG, Wiederhorn SM (1974a) Proof testing of ceramic materials-an analytical basis for failure prediction. Int J Fract 10(3):379–392

Evans AG, Wiederhorn SM (1974b) Crack propagation and failure prediction in silicon nitride at elevated temperature. J Mater Sci 9(2):270–278

Evans AG, Russell LR, Richerson DW (1975) Slow crack growth in ceramic materials at elevated temperatures. Metall Mater Trans A 6:707–716

Gilberta CJ, Ritchiea RO (1998) Transient fatigue-crack growth behavior following variable-amplitude loading in a monolithic silicon nitride ceramic. Eng Fract Mech 60(3):303–313

Guiu F, Reece MJ, Vaughan DAJ (1991) Cyclic fatigue of ceramics. J Mater Sci 26:3275–3286

Hasselman DPH, Chen EP, Ammann CL, Doherty JE, Nessler CG (1975) Failure prediction of the thermal fatigue of silicon nitride. J Am Ceram Soc 58(11–12):513–516

Hoshide T, Hiramatsu H (1999) A microstructural approach to flaw size dependence of strength in engineering ceramics. Fatig Fract Eng Mater Struct 22(12):1029–1039

Hoshide T, Ohara T, Yamada T (1988) Fatigue behavior of ceramic materials under variable stress amplitude. Eng Fract Mech 31(2):339–347

Kamiya N, Kamigaito O (1982) Thermal fatigue life of ceramics under mechanical load. J Mater Sci 17(11):3149–3157

Matsuda S (2016) Fracture characteristics of silicon nitride ceramic ball subjected to thermal shock. J Mater Sci 51(11):5502–5513

Matsuda S, Ogi K (2017) Effect analysis of loading rate on relationship between strength and flaw size of ceramics using probabilistic model on the basis of SCG concept. Trans JSME 83(847):16–00369

Matsuda S, Watanabe R (2011) Estimation of dynamic fatigue strengths in brittle materials under a wide range of stress rates. J Mater Sci 46(15):5056–5063

Ogi K, Ito K (2011) A probabilistic approach for thermal shock fatigue life of glass. Fatigue Fract Eng Mater Struct 34(9):643–653

Ogi K, Yashiro S, Niimi K (2010) A probabilistic approach for transverse crack evolution in a composite laminate under variable amplitude cyclic loading. Compos A 41(3):383–390

Okabe N, Ikeda T (1991) Strength evaluation method and design optimization for ceramic gas turbine blades. Mater Sci Eng A 143(1–2):11–19

Pan LS, Matsuzawa M, Horibe S (1998) Stress rate dependence of fracture strength in pre-cracked zirconia ceramics. Mater Sci Eng A 244(2):199–206

Pfingsten T, Glien K (2006) Statistical analysis of slow crack growth experiments. J Eur Ceram Soc 26(15):3061–3065

Phani KK (1988) Analysis of static and dynamic fatigue of polycrystalline alumina. J Mater Sci 23(11):3864–3868

Quinn GD, Salem J, Bar-on I, Cho K, Foley M, Fang H (1992) Fracture toughness of advanced ceramics at room temperature. J Res Natl Inst Stand Technol 97(5):579–607

Ritter JE (1995) Predicting lifetimes of materials and material structures. Dent Mater 11(2):142–146

Ritter JE Jr, Humenik JN (1979) Static and dynamic fatigue of polycrystalline alumina. J Mater Sci 14(3):626–632

Sakai T, Tanaka T (1980) Estimation of three parameters of Weibull distribution in relation to parameter estimation of fatigue life distribution: continued report. J Soc Mater Sci Jpn 29(316):17–23

Seshadri SG, Srinivasan M, Weber GW (1982) Evaluation of slow crack growth parameters for silicon carbide ceramics. J Mater Sci 17(5):1297–1302

Siegmund T (2004) A numerical study of transient fatigue crack growth by use of an irreversible cohesive zone model. Int J Fatigue 26(9):929–939

Tanaka T, Nakayama H, Okabe N, Yamamoto S, Fukui S (2002) Creep rupture map of engineering fine ceramics. In: Bradt RC et al (eds) Fracture mechanics of ceramics, vol 10. Plenum Press, New York, pp II-308–II-326

Teixeira EC, Piascik JR, Stoner BR, Thompson JY (2007) Dynamic fatigue and strength characterization of three ceramic materials. J Mater Sci Mater M 18(6):1219–1224

To T, Célarié F, Roux-Langlois C, Bazin A, Gueguen Y, Orain H, Le Fur M, Burgaud V, Rouxel T (2018) Fracture toughness, fracture energy and slow crack growth of glass as investigated by the single-edge precracked beam (SEPB) and chevron-notched beam (CNB) methods. Acta Mater 146:1–11

Usami S, Kimoto H, Takahashi I, Shida S (1986) Strength of ceramic materials containing small flaws. Eng Fract Mech 23(4):745–761

Wiederhorn SW, Bolz LH (1970) Stress corrosion and static fatigue of glass. J Am Ceram Soc 53(10):543–548

Zhu P, Lin Z, Chen G, Ikeda K (2004) The predictions and applications of fatigue lifetime in alumina and zirconia ceramics. Int J Fatigue 26(10):1109–1114